Wafer Scale Homogeneous Bilayer Graphene Films by Chemical Vapor Deposition

Seunghyun Lee,[†] Kyunghoon Lee,[†] and Zhaohui Zhong*

Department of Electrical Engineering and Computer Science, University of Michigan, Ann Arbor, Michigan 48109, United States

ABSTRACT The discovery of electric field induced band gap opening in bilayer graphene opens a new door for making semiconducting graphene without aggressive size scaling or using expensive substrates. However, bilayer graphene samples have been limited to μm^2 size scale thus far, and synthesis of wafer scale bilayer graphene poses a tremendous challenge. Here we report homogeneous bilayer graphene films over at least a 2 in. × 2 in. area, synthesized by chemical vapor deposition on copper foil and subsequently transferred to arbitrary substrates. The bilayer nature of graphene film is verified by Raman spectroscopy, atomic force microscopy, and transmission electron microscopy. Importantly, spatially resolved Raman spectroscopy confirms a bilayer coverage of over 99%. The homogeneity of the film is further supported by electrical transport measurements on dual-gate bilayer graphene transistors, in which a band gap opening is observed in 98% of the devices.

KEYWORDS Graphene, bilayer, chemical vapor deposition, wafer scale, band gap opening

Single and few-layer graphene[1−5] are promising materials for post-silicon electronics because of their potential of integrating bottom-up nanomaterial synthesis with top-down lithographic fabrication at wafer scale.[4,6] However, single-layer graphene is intrinsically semimetal; introducing an energy band gap requires patterning nanometer-width graphene ribbons[7−9] or utilizing special substrates.[10−12] Bilayer graphene, instead, has an electric field induced band gap up to 250 meV,[13−18] thus eliminating the need for extreme scaling or costly substrates. Furthermore, exciton binding energies in bilayer graphene are also found to be tunable with an electric field.[19] The unique ability of controlling the band gap and the exciton energy can lead to new possibilities of bilayer graphene based electronics and photonics.

To date, most bilayer graphene samples are fabricated using mechanical exfoliation of graphite,[15−18] which have limited sizes of μm^2 and are certainly not scalable. Recent developments in chemical vapor deposition (CVD) methods have allowed successful production of large scale single-layer graphene on metal substrate.[20−24] However, the synthesis of uniform bilayer graphene film remains extremely challenging. Here we report the first synthesis of wafer scale bilayer graphene film over at least 2 in. × 2 in. area, limited only by our synthesis apparatus. Our method is based on CVD growth of bilayer graphene on a copper surface and is characterized by the depletion of hydrogen, high vacuum, and, most importantly, slower cooling rate compared to previous single-layer graphene synthesis.[21,22,24] The optimal

bilayer graphene film is grown at 1000 °C for 15 min, with growth pressure of 0.5 Torr, CH_4 flow rate of 70 sccm, and a cooling rate of 18 °C/min (0.3 °C/s) (Figure S1 in the Supporting Information).

Figure 1a shows photographic image of a wafer scale (2 in. × 2 in.) bilayer graphene film transferred onto a 4 in. silicon wafer with 280 nm thick SiO_2. A typical optical microscope image (Figure 1b) of the transferred bilayer graphene film shows almost no color variation except for
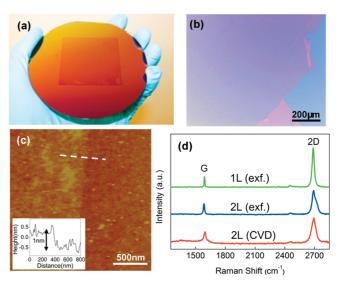

FIGURE 1. Wafer scale homogeneous bilayer graphene film grown by CVD. (a) Photograph of a 2 in. × 2 in. bilayer graphene film transferred onto a 4 in. Si substrate with 280 nm thermal oxide. (b) Optical microscopy image showing the edge of a bilayer graphene film. (c) AFM image of patterned bilayer graphene transferred onto SiO_2/Si substrate. (Inset) Cross section height profile measured along the dotted line. (d) Raman spectra taken from CVD grown bilayer graphene (red solid line), exfoliated single-layer (green solid line), and bilayer graphene (blue solid line) samples. Laser excitation wavelength is 514 nm.

* Corresponding author, zzhong@umich.edu.

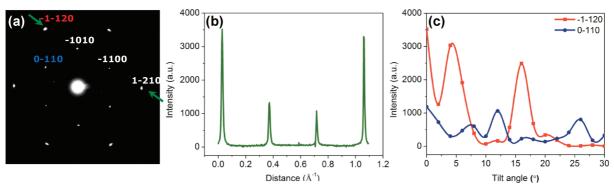† These authors contributed equally to this work.

FIGURE 2. Selected area electron diffraction pattern of bilayer graphene. (a) Normal incident diffraction pattern of bilayer graphene sample. The bilayer graphene film was transferred onto copper grid with holey carbon supporting film. The diffraction image was taken by a JEOL 2010F analytical electron microscope with acceleration voltage of 200 kV. (b) Profile plot of diffraction peak intensities across a line cut indicated by the green arrows shown in (a). (c) Diffraction peak intensities as a function of tilt angle for (0−110) (in blue) and (−1−120) (in red).

the region where the film is torn and folded (lower right of Figure 1b). To identify the number of layers for our graphene sample, the film thickness is first measured using atomic force microscopy (AFM (Figure 1c). Height profiles across patterned graphene edges show that thickness of our graphene samples ranges from 0.9 to 1.3 nm, suggesting the number of graphene layers below 3.[23]

We further performed Raman spectroscopy measurements (Renishaw spectrometer at 514 nm) on 10 randomly chosen spots across the film and compared them with reference samples prepared by mechanically exfoliating Kish graphite.[17,25,26] The red curve in Figure 1c represents a typical Raman spectrum from our sample. Two peaks are clearly visible between a Raman shift of 1250−2850 cm^{-1}, corresponding to the G band (~1595 cm^{-1}) and 2D band (~2691 cm^{-1}), respectively.[26−30] Importantly, the spectrum exhibits several distinctive features. First, the 2D band shows a higher peak intensity than the G band with a 2D-to-G intensity ratio $I_{2D}/I_G \sim 2.31$, suggesting the number of graphene layers less than 3.[24,27,29] Second, the full width at half-maximum (fwhm) of the 2D band peak is measured to be ~45 cm^{-1}, exceeding the cutoff of ~30 cm^{-1} for single-layer graphene.[25,26,28] Third, the 2D band peak cannot be fitted with single Lorentzian (Figure S2a in the Supporting Information), but fitting from four Lorentzian peaks with a fwhm of 24 cm^{-1} yields excellent agreement (Figure S2b in the Supporting Information).[26−28] Raman spectra taken from the other nine spots show similar features with the 2D band fwhm of 43−53 cm^{-1}. These observations are strongly reminiscent of the characteristic bilayer graphene Raman spectrum. In addition, reference Raman spectra taken under identical conditions from exfoliated single-layer (green curve) and bilayer (blue curve) graphene are also presented in Figure 1c. Exfoliated single-layer graphene shows a 2D band fwhm of 24 cm^{-1} and I_{2D}/I_G of 3.79, while exfoliated bilayer graphene shows a fwhm of 46 cm^{-1} and I_{2D}/I_G of 2.25. Together, the AFM height measurements, the Raman spectra, and the direct comparison with the exfoliated samples clearly support the bilayer nature of our CVD synthesized

graphene film. We also measured the D band to G band intensity ratio, I_D/I_G, of our bilayer graphene sample to be around 0.11−0.3, indicating a relatively low defect density.

A transmission electron microscopy (TEM) selected area electron diffraction pattern was measured to further characterize the graphene film (Figure 2a). The 6-fold symmetry is clearly visible and Bravais−Miller (*hkil*) indices are used to label the diffraction peaks. Importantly, the diffraction intensities of inner peaks from equivalent planes {1100} are always higher than outer peaks from {2100}. The intensity ratios of I_{-1010}/I_{-1-120} and I_{-1100}/I_{1-210} are close to 0.28 (Figure 2b), indicating that the film is not a single layer and it retains AB stacking structure.[31−33] We further studied the tilt-angle-dependent diffraction peak intensity for both inner and outer peaks. As shown in Figure 2c, both (0−110) and (−1−120) peaks show strong intensity modulation with tilt angle, and both peaks can be suppressed completely at a certain angle. It is known that monolayer graphene has only a zero order Laue zone and weak intensity modulation is expected at any angle.[32,33] Our TEM results again agree with AFM and Raman measurements for the bilayer nature of the graphene film. We also notice additional diffraction spots, which are caused by the residues on the film due to insufficient sample cleaning.

To further evaluate the uniformity of CVD grown bilayer graphene film, we performed spatially resolved Raman spectroscopy. Here, identification of the number of graphene layers relies on a combination of the fwhm of the 2D band[24,26−28,30] and peak intensity ratio I_{2D}/I_G.[23,24,27,29] Figure 3a shows a color map of the 2D band peak width over 30 μm by 30 μm area, with fwhm values ranging from 42 cm^{-1} (dark color) to 63 cm^{-1} (bright yellow). The data show uniformly distributed red color with only a few localized yellow spots. The peak intensity ratios I_{2D}/I_G are also mapped in color (Figure 3b) over the same area, with values ranging from 0.37 (dark color) to 3.77 (bright yellow). Comparisons between Figure 3a and Figure 3b reveal that larger peak widths are consistent with smaller I_{2D}/I_G ratios. Furthermore, Figure 3c compares the Raman spectra taken from three
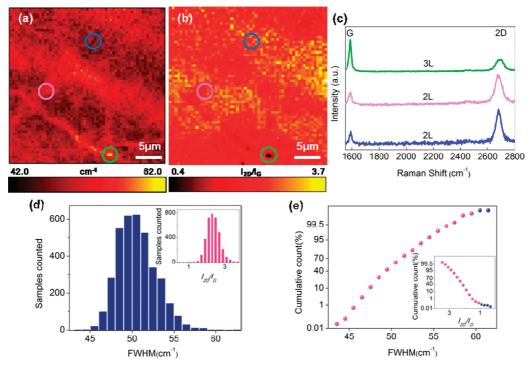
FIGURE 3. Spatially resolved Raman spectroscopy of CVD bilayer graphene. (a) and (b) Two-dimensional color mapping of the fwhm's of Raman 2D band and I_{2D}/I_G ratios over a 30 μm × 30 μm area, respectively. (c) Raman spectra from the marked spots corresponding colored circles showing bilayer and trilayer graphene. (d) Histogram of the fwhm's of Raman 2D band corresponding to area shown in (a). (top right inset) Histogram of I_{2D}/I_G ratios for the same area. (e) Cumulative count plot of fwhm's of 2D band. Pink (blue) spheres represent the fwhm less (more) than 60 cm^{-1}. (inset) Cumulative count plot of I_{2D}/I_G ratios. Pink (blue) spheres indicate the ratio larger (smaller) than 1. (For Raman mapping, λ_{laser} = 514 nm, 500 nm step size, 100× objector.)

representative spots indicated using green, pink, and blue circles. The Raman spectrum taken at green-circled spot has the largest fwhm (62.9 cm^{-1}) and smallest I_{2D}/I_G (0.37), indicating trilayer graphene (Figure S2c in the Supporting Information); the pink-circled (blue-circled) spot shows fwhm =55 cm^{-1} and I_{2D}/I_G = 2.2 (fwhm = 43.8 cm^{-1} and I_{2D}/I_G = 2.91), indicating bilayer graphene. These results confirm that the CVD bilayer graphene film is highly homogeneous, with only a very small fraction corresponding to possibly three layers.

We then quantified the bilayer graphene coverage by studying the statistics of 2D band peak width and I_{2D}/I_G ratio. Figure 3d illustrates the histogram of the fwhm's of 2D band taken from the Raman mapping. The average peak width is determined to be 51 ± 2 cm^{-1}. Furthermore, cumulative counts plotted in Figure 3e indicate that more than 99 % of the fwhm values are below 60 cm^{-1} (pink spheres). In addition, the histogram of I_{2D}/I_G ratios (Figure 3d, inset) shows an average value of 2.4 ± 0.4, and the corresponding cumulative count plot (Figure 3e, inset) shows that more than 99 % of I_{2D}/I_G ratios are larger than 1. Using fwhm = 60 cm^{-1} together with I_{2D}/I_G = 1 as the crossover values between bilayer and trilayer graphene, our data give an estimate of at least 99 % coverage of bilayer graphene with less than 1 % of trilayer over the entire area.

A direct verification of the bilayer nature of our CVD graphene film comes from electrical transport measure-

ments. For this purpose, dual-gate bilayer graphene transistors were fabricated with three different dimensions, channel lengths and channel widths of 1 μm × 1 μm, 1 μm × 2 μm, and 2 μm × 2 μm, respectively. A scanning electron microscope (SEM) image and an illustration of the fabricated device are shown in Figure 4a. All devices have a local top gate and a universal silicon bottom gate with Al$_2$O$_3$ (40 nm) and SiO$_2$ (310 nm) as the respective gate dielectrics. This dual-gate structure allows simultaneous manipulation of bilayer graphene band gap and the carrier density by independently inducing electric fields in both directions.[15,16]

Figure 4b shows a two-dimensional color plot of square resistance $R_\square$ vs both top gate voltage (V_{tg}) and bottom gate voltage (V_{bg}), obtained from a typical 1 × 1 μm device at 6.5 K. The red and blue colors represent high and low square resistance, respectively. The data clearly show that $R_\square$ reach peak values along the diagonal (red color region), indicating a series of charge neutral points (Dirac points) when the top displacement fields cancel out the bottom displacement fields.[15,16] More importantly, the peak square resistance, $R_{\square,Dirac}$, reaches maximum at the upper left and lower right corners of the graph, where the average displacement fields from top and bottom gates are largest. Horizontal section views of the color plot in Figure 4b are also shown in Figure 4c, with $R_\square$ plotted against V_{tg} at fixed V_{bg} from −100 to 140 V. Once again, for each $R_\square$ vs V_{tg} curve square resistances exhibit a peak value, and $R_{\square,Dirac}$ increases with increasing
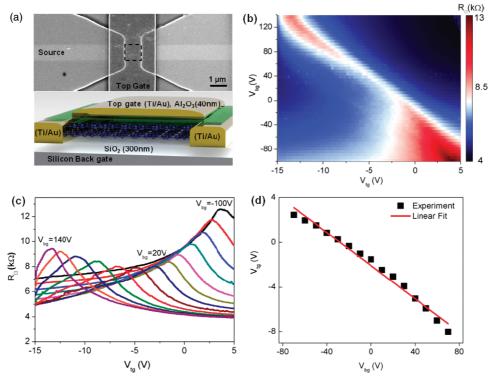
FIGURE 4. Electrical transport studies on dual-gate bilayer graphene devices. (a) Scanning electron microscopy image (top) and illustration (bottom) of a dual-gate bilayer device. The dashed square in the SEM image indicates the 1 μm × 1 μm bilayer graphene piece underneath the top gate. (b) Two-dimensional color plot of square resistance $R_\square$ vs top gate voltage V_{tg} and back gate voltage V_{bg} at temperature of 6.5K. (c) $R_\square$ vs V_{tg} at different value of fixed V_{bg}. The series of curves are taken from V_{bg} of −100 to 140 V, with 20 V increment. (d) The charge neutral points indicated as set of (V_{tg}, V_{bg}) values at the peak square resistance $R_{\square,dirac}$. The red line is the linear fit. The electrical measurements were carried out in a closed cycle cryogenic probe station (LakeShore, CRX-4K), using a lock-in technique at 1kHz with ac excitation voltage of 100 μV.

V_{bg} in both a positive and negative direction. The charge neutral points are further identified in Figure 4d in terms of the (V_{tg}, V_{bg}) values at $R_{\square,Dirac}$. A linear relation between V_{tg} and V_{bg} is observed with a slope of −0.073, which agrees with the expected value of $-\varepsilon_{bg}d_{tg}/\varepsilon_{tg}d_{bg} = -0.067$, where ε and d correspond to the dielectric constant and thickness of the top gate (Al_2O_3: $d_{tg} = 40$ nm, $\varepsilon_{tg} = 7.5$) and bottom gate (SiO_2: $d_{bg} = 310$ nm, $\varepsilon_{bg} = 3.9$) oxide.[15,16] We also notice the deviation from linear relation at high field; the origin of which is not understood currently and requires further study.

Similar results from three other devices are shown in Figure S3 in the Supporting Information, and more than 46 measured devices show qualitative agreement. These electrical characterizations yield direct evidence for the successful synthesis of bilayer graphene. The observation of increasing $R_{\square,Dirac}$ values at higher fields is an unmistakable sign of band gap opening in bilayer graphene.[15,16] In comparison, the peak resistance at the charge neutral point should remain roughly constant for single-layer graphene,[15] while $R_{\square,Dirac}$ decreases at higher field for trilayer graphene.[5] In addition, we also compared the temperature dependence of $R_{\square,Dirac}$ at $V_{bg} \sim 0$ V and $V_{bg} \sim -100$ V (Figure S5 in the Supporting Information). Larger variation of $R_{\square,Dirac}$ vs temperature is observed under higher electric field, which again agrees with field-induced band gap opening in bilayer graphene.[15,16] We

note that the observed resistance modulation due to electric field and temperature are smaller compared to devices made by mechanical exfoliation,[15,16] which can be attributed to the polycrystalline nature of CVD graphene film. We also note that our devices show large fluctuations of the offset voltage (from impurity and surface doping), with some cases exceeding 140 V for the bottom gate. This could be caused by the ion residues from the etching process, and further investigations are needed.

We also studied the statistics of bilayer graphene occurrence for 63 (7 row × 9 columns) dual-gate devices fabricated across the same film (Figure 5a). Forty six out of 63 devices show bilayer graphene behaviors, characterized by increasing $R_{\square,Dirac}$ at larger fields. Of the remaining devices, two devices contain no graphene pieces, and 14 devices have fabrication defects (see Supporting Information). Interestingly, one device shows trilayer characteristics[5] with decreasing $R_{\square,Dirac}$ under both more positive and more negative fields (Figure S4 in the Supporting Information). Hence, 46 out of 47 (98%) working devices show bilayer characteristics. For the bilayer graphene devices, we also calculated the maximum percentage changes of peak square resistance, $\Delta R_{\square,Dirac}/R_{\square,Dirac,min}$, in which $\Delta R_{\square,Dirac}$ denotes the maximum difference in $R_{\square,Dirac}$ within V_{tg} of ±10 V and V_{bg} of ±120 V, and $R_{\square,Dirac,min}$ is the minimum peak square
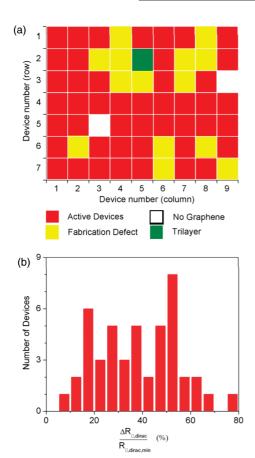
FIGURE 5. Bilayer statistics from electrical transport measurement on dual-gate graphene devices. (a) A color-coded map of 63 devices (7 rows × 9 columns) fabricated across the same graphene film. The red squares indicate bilayer graphene confirmed by transport measurement, the yellow squares indicate devices which have fabrication defects, the white squares mark the region with no graphene, and the green square represents a device with trilayer response from the transport measurement. (b) Histogram of $\Delta R_{\square,\text{Dirac}}/R_{\square,\text{Dirac,min}}$ values in percentage for 46 active devices. $\Delta R_{\square,\text{Dirac}}$ corresponds to the maximum difference in $R_{\square,\text{Dirac}}$ within V_{tg} of ± 10 V and V_{bg} of ± 120 V. $R_{\square,\text{Dirac,min}}$ is the minimum peak resistance.

resistance. A histogram of the percentile changes is shown in Figure 5b, with an average peak resistance change of 38 % and maximum value of 77 %. In addition, the average room temperature carrier mobilities were measured to be ~580 cm^2 V^{-1} s^{-1}, which are the lower-bound values without excluding the device contact resistance. The smaller-than-expected $R_{\square,\text{Dirac}}$ modulation is believed to be caused by defects and unintended impurity doping.[16] High-quality gate dielectrics have been shown to improve the bilayer graphene device performance dramatically.[18] The electrical measurement results echo the finding from Raman measurements: our CVD grown bilayer graphene film is highly homogeneous.

Lastly, we would like to comment on the key growth parameters for our CVD bilayer graphene films. It has been suggested that graphene growth on the copper surface is self-limited to a single layer,[24] but both of our Raman and electrical characterizations clearly prove otherwise. We systematically varied the key growth conditions, and the

resulting film quality was evaluated using Raman spectroscopy (Table S1 in the Supporting Information). In brief, increasing CH$_4$ flow rate by 2 times has no noticeable effect on 2D bandwidth and $I_{\text{2D}}/I_{\text{G}}$ values, except for a larger $I_{\text{D}}/I_{\text{G}}$ ratio corresponding to more disorders. However, increasing growth pressure to ambient condition leads to larger 2D bandwidth and smaller $I_{\text{2D}}/I_{\text{G}}$ ratio, indicating the increasing portion of trilayer graphene. This result is consistent with recent literature that higher pressure favors multilayer graphene growth on copper surface.[34] On the basis of our results, we speculate that the key parameter for the bilayer graphene film growth is the slow cooling process (~18 °C/min). Cooling rate has been found to be the critical factor for forming uniform single or bilayer graphene on nickel.[21,35,36] Our initial results should promote studies of the detailed growth mechanism for bilayer graphene.

The size of the homogeneous bilayer graphene films is limited only by the synthesis apparatus, which can be further scaled up. The integration with existing top-down lithography techniques should bring significant advancement for high-performance, lightweight, and transparent graphene electronics and photonics. Furthermore, because the CVD grown bilayer graphene film can be transferred to arbitrary substrates, adopting high-k dielectrics for both top and bottom gates should drastically improve the device performance.[18] A few voltages applied to the gate electrodes will be able to open up a sizable band gap (~250 meV).

Supporting Information Available. Growth and transfer process, device fabrication, a table of key growth parameters, figures for Lorentzian fitting of Raman spectrum, additional two-dimensional color plot of bilayer electrical transport and trilayer electrical transport characteristics, and temperature-dependent resistance change. This material is available free of charge via the Internet at http://pubs.acs.org.

REFERENCES AND NOTES

(1) Geim, A. K.; Novoselov, K. S. *Nat. Mater.* **2007**, *6*, 183–191.
(2) Castro Neto, A. H.; Guinea, F.; Peres, N. M. R.; Novoselov, K. S.; Geim, A. K. *Rev. Mod. Phys.* **2009**, *81*, 109.
(3) Geim, A. K. *Science* **2009**, *324*, 1530–1534.
(4) Schwierz, F. *Nat. Nanotechnol.* **2010**, *5*, 487–496.
(5) Craciun, M. F.; Russo, S.; Yamamoto, M.; Oostinga, J. B.; Morpurgo, A. F.; Tarucha, S. *Nat. Nanotechnol.* **2009**, *4*, 383–388.
(6) Lin, Y.-M.; Dimitrakopoulos, C.; Jenkins, K. A.; Farmer, D. B.; Chiu, H.-Y.; Grill, A.; Avouris, P. *Science* **2010**, *327*, 662.
(7) Han, M. Y.; Özyilmaz, B.; Zhang, Y.; Kim, P. *Phys. Rev. Lett.* **2007**, *98*, 206805.

(8) Chen, Z.; Lin, Y.-M.; Rooks, M. J.; Avouris, P. *Physica E* **2007**, *40*, 228–232.

(9) Li, X. L.; Wang, X. R.; Zhang, L.; Lee, S. W.; Dai, H. J. *Science* **2008**, *319*, 1229–1232.

(10) Zhou, S. Y.; Gweon, G. H.; Fedorov, A. V.; First, P. N.; de Heer, W. A.; Lee, D. H.; Guinea, F.; Castro Neto, A. H.; Lanzara, A. *Nat. Mater.* **2007**, *6*, 770–775.

(11) Ohta, T.; Bostwick, A.; Seyller, T.; Horn, K.; Rotenberg, E. *Science* **2006**, *313*, 951–954.

(12) Sutter, P. W.; Flege, J.-I.; Sutter, E. A. *Nat. Mater.* **2008**, *7*, 406–411.

(13) McCann, E. *Phys. Rev. B* **2006**, *74*, 161403.

(14) Castro, E. V.; Novoselov, K. S.; Morozov, S. V.; Peres, N. M. R.; dos Santos, J. M. B. L.; Nilsson, J.; Guinea, F.; Geim, A. K.; Neto, A. H. C. *Phys. Rev. Lett.* **2007**, *99*, 216802.

(15) Oostinga, J. B.; Heersche, H. B.; Liu, X.; Morpurgo, A. F.; Vandersypen, L. M. K. *Nat. Mater.* **2008**, *7*, 151–157.

(16) Zhang, Y.; Tang, T.-T.; Girit, C.; Hao, Z.; Martin, M. C.; Zettl, A.; Crommie, M. F.; Shen, Y. R.; Wang, F. *Nature* **2009**, *459*, 820–823.

(17) Mak, K. F.; Lui, C. H.; Shan, J.; Heinz, T. F. *Phys. Rev. Lett.* **2009**, *102*, 256405.

(18) Xia, F.; Farmer, D. B.; Lin, Y.-m.; Avouris, P. *Nano Lett.* **2010**, *10*, 715–718.

(19) Park, C.-H.; Louie, S. G. *Nano Lett.* **2010**, *10*, 426–431.

(20) Coraux, J.; N'Diaye, A. T.; Busse, C.; Michely, T. *Nano Lett.* **2008**, *8*, 565–570.

(21) Kim, K. S.; Zhao, Y.; Jang, H.; Lee, S. Y.; Kim, J. M.; Kim, K. S.; Ahn, J.-H.; Kim, P.; Choi, J.-Y.; Hong, B. H. *Nature* **2009**, *457*, 706–710.

(22) Lee, Y.; Bae, S.; Jang, H.; Jang, S.; Zhu, S.-E.; Sim, S. H.; Song, Y. I.; Hong, B. H.; Ahn, J.-H. *Nano Lett.* **2010**, *10*, 490–493.

(23) Reina, A.; Jia, X.; Ho, J.; Nezich, D.; Son, H.; Bulovic, V.; Dresselhaus, M. S.; Kong, J. *Nano Lett.* **2008**, *9*, 30–35.

(24) Li, X.; Cai, W.; An, J.; Kim, S.; Nah, J.; Yang, D.; Piner, R.; Velamakanni, A.; Jung, I.; Tutuc, E.; Banerjee, S. K.; Colombo, L.; Ruoff, R. S. *Science* **2009**, *324*, 1312–1314.

(25) Berciaud, S. p.; Ryu, S.; Brus, L. E.; Heinz, T. F. *Nano Lett.* **2008**, *9*, 346–352.

(26) Malard, L. M.; Pimenta, M. A.; Dresselhaus, G.; Dresselhaus, M. S. *Phys. Rep.* **2009**, *473*, 51–87.

(27) Ferrari, A. C.; Meyer, J. C.; Scardaci, V.; Casiraghi, C.; Lazzeri, M.; Mauri, F.; Piscanec, S.; Jiang, D.; Novoselov, K. S.; Roth, S.; Geim, A. K. *Phys. Rev. Lett.* **2006**, *97*, 187401.

(28) Graf, D.; Molitor, F.; Ensslin, K.; Stampfer, C.; Jungen, A.; Hierold, C.; Wirtz, L. *Nano Lett.* **2007**, *7*, 238–242.

(29) Gupta, A.; Chen, G.; Joshi, P.; Tadigadapa, S.; Eklund, *Nano Lett.* **2006**, *6*, 2667–2673.

(30) Hao, Y.; Wang, Y.; Wang, L.; Ni, Z.; Wang, Z.; Wang, R.; Koo, C. K.; Shen, Z.; Thong, J. T. L. *Small* **2010**, *6*, 195–200.

(31) Horiuchi, S.; Gotou, T.; Fujiwara, M.; Sotoaka, R.; Hirata, M.; Kimoto, K.; Asaka, T.; Yokosawa, T.; Matsui, Y.; Watanabe, K.; Sekita, M. *Jpn. J. Appl. Phys.* **2003**, *42*, L1073.

(32) Meyer, J. C.; Geim, A. K.; Katsnelson, M. I.; Novoselov, K. S.; Obergfell, D.; Roth, S.; Girit, C.; Zettl, A. *Solid State Commun.* **2007**, *143*, 101–109.

(33) Meyer, J. C.; Geim, A. K.; Katsnelson, M. I.; Novoselov, K. S.; Booth, T. J.; Roth, S. *Nature* **2007**, *446*, 60–63.

(34) Bhaviripudi, S.; Jia, X.; Dresselhaus, M. S.; Kong, J. *Nano Lett.* **2010**, *10*, 4128–4133.

(35) Yu, Q. K.; Lian, J.; Siriponglert, S.; Li, H.; Chen, Y. P.; Pei, S. S. *Appl. Phys. Lett.* **2008**, *93*, 113103.

(36) Reina, A.; Thiele, S.; Jia, X.; Bhaviripudi, S.; Dresselhaus, M.; Schaefer, J.; Kong, J. *Nano Res.* **2009**, *2*, 509–516.